iScience

CellPress
OPEN ACCESS

Article

Synthesis, characterization, and application of thio-salicylaldehyde schiff base complexes for Cr (VI) adsorption

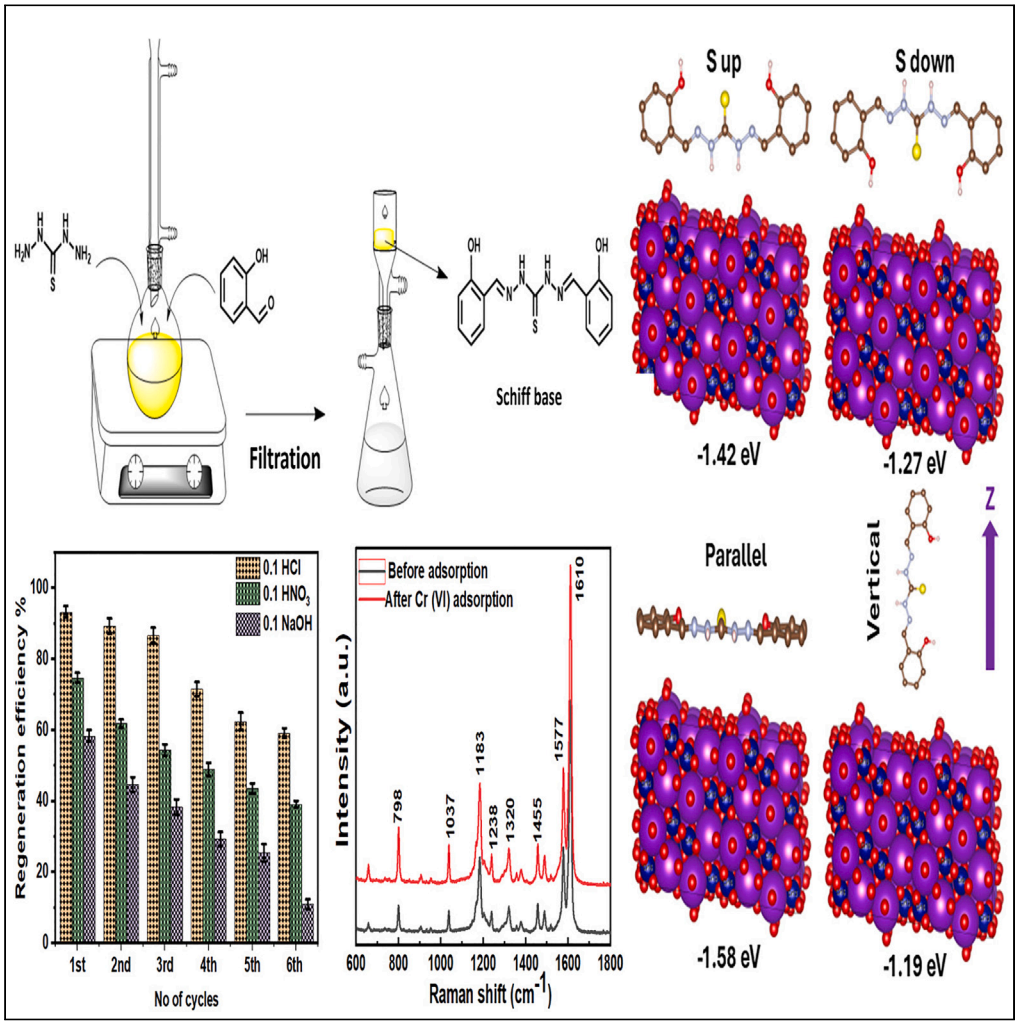

Simranjeet Singh, Shweta Shekar, Sushant K. Behera, Nabila Shehata, Nadeem A. Khan, Joginder Singh, Praveen C. Ramamurthy

onegroupb203@gmail.com

Highlights

Schiff base produced from thio-carbohydrazide and salicylaldehyde for Cr (VI) removal

Adsorption data supported by experimental and DFT studies

Data fitted by the Avrami model and Freundlich isotherms

Regeneration capability of up to six cycles

Singh et al., iScience 27, 110925
October 18, 2024
Published by Elsevier Inc.
https://doi.org/10.1016/j.isci.2024.110925

iScience

CellPress
OPEN ACCESS

Article

Synthesis, characterization, and application of thio-salicylaldehyde schiff base complexes for Cr (VI) adsorption

Simranjeet Singh,[1] Shweta Shekar,[2] Sushant K. Behera,[2] Nabila Shehata,[3] Nadeem A. Khan,[4] Joginder Singh,[5] and Praveen C. Ramamurthy[1,6,*]

SUMMARY

This study investigates the effectiveness of a Schiff base derived from thio-carbohydrazide and salicylaldehyde as an adsorbent for Cr(VI) removal from wastewater. The Schiff base demonstrated excellent adsorption capacity and reusability, with high removal efficiency and rapid adsorption kinetics. The results were supported by theoretical density functional theory simulations, which revealed the enhanced dynamic nature of the Schiff base system for heavy metal adsorption. These findings highlight the potential of Schiff base complexes as sustainable and efficient adsorbents for industrial wastewater treatment.

INTRODUCTION

The global increase in industrialization and urbanization has significantly damaged our aquatic environment due to the release of industrial and domestic pollution. These effluents often contain high levels of harmful heavy metals which are then released into the surrounding aquatic and terrestrial ecosystems.[1] Given the carcinogenic and mutagenic properties, Cr (VI) is unique among heavy metals.[2,3] Effective and long-term remediation strategies are now being sought to alleviate the negative effects on human health and ecological systems. Both chromate (CrO_4^{2-}) and dichromate ($Cr_2O_7^{2-}$) which are common Cr (VI) anions have significant oxidizing properties. Chromate is a confirmed carcinogen and is also suspected to be a mutagen and teratogen in biological systems. The United States Environmental Protection Agency (US EPA) mandates that the concentration of Cr (VI) in drinking water must not exceed 0.05 mg/L, and for inland surface waters, the limit is 0.1 mg/L.[4] Therefore, it is essential to treat wastewater containing chromium to reduce the concentration of Cr (VI) to permissible levels before discharging it into the environment.

Among the conventional processes used to remove Cr (VI), reduction and precipitation as chromium hydroxide are the most commonly applied methods. However, these methods are often associated with relatively high operational costs. Consequently, there is a need to develop a more cost-effective alternative technology that can complement the existing methods. Adsorption is one of the most promising approaches for managing heavy metals in synthetic wastewater due to its simplicity, effectiveness, and efficiency. The use of Schiff-base complexes as adsorbents to eliminate Cr (VI) has recently captured significant attention within the scientific community.[5,6] These Schiff bases, originating from the condensation of ketones or aldehydes with primary amines, exhibit versatile structures and tuneable properties, rendering them appealing candidates for the chelation and adsorption of metal ions.[5,7–11] The interaction between Schiff-base complexes and Cr (VI) ions provides an avenue for the novel exploration involving various factors such as complex formation mechanisms, adsorption kinetics, thermodynamics, and the influence of different environmental factors. Optimizing the design and synthesis of tailor-made Schiff-base ligands can enhance the absorptive capacity, selectivity, and stability of the resulting complexes.

The primary objective of this study is to provide a comprehensive examination of the chemical reaction rates and the complexation processes involved in the adsorption of Cr (VI). This adsorption is facilitated by a Schiff base derived from thio-carbohydrazide and salicylaldehyde. The study includes a detailed overview of the fundamental principles of adsorption, the synthesis of the Schiff base adsorbent, and the characterization techniques used to elucidate the interaction between ions and the Schiff base. Additionally, the study thoroughly examines the various factors influencing the adsorption process, including pH, temperature, and ion concentration. The adsorption isotherm modeling was discussed using non-linear models, such as Freundlich, Langmuir, Dubinin–Radushkevich, Langmuir-Freundlich, Sips, Temkin, Redlich-Peterson, Toth, Khan, Baudu, and Fritz-Schlunder. Moreover, the adsorption kinetics were evaluated using five models: Pseudo-1st-order, Pseudo-2nd-order, mixed 1st and 2nd-order, and Avrami models. The novelty of this work lies in its insights into the specific interactions

[1]Interdisciplinary Centre for Water Research (ICWaR), Indian Institute of Science, Bangalore 560012, India
[2]Department of Materials Engineering, Indian Institute of Science, Bangalore 560012, India
[3]Environmental Science and Industrial Development Department, Faculty of Postgraduate Studies for Advanced Sciences, Beni-Suef University, Beni-Suef, Egypt
[4]Interdisciplinary Research Center for Membranes and Water Security, King Fahd University of Petroleum and Minerals, Dhahran 31261, Saudi Arabia
[5]Department of Botany, Nagaland University, HQRS: Lumami, Lumami, Nagaland 798627, India
[6]Lead contact
*Correspondence: onegroupb203@gmail.com
https://doi.org/10.1016/j.isci.2024.110925

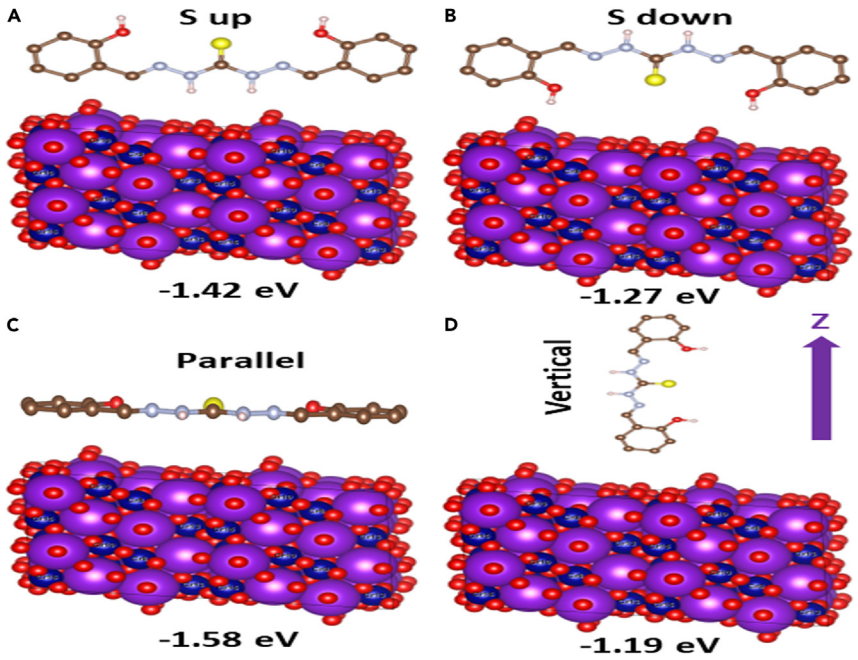

Figure 1. Optimized adsorption of Cr (VI) by TSA Schiff's base: energy configurations in different orientations

Optimized structures with the calculated Cr (VI) adsorption configurations of TSA Schiff's base molecule along *S*-up (A), *S*-down (B), parallel (C), and vertical (D) orientations along *z* axis of the surfaces. The calculated adsorption energies are mentioned with van der Waals corrections.

between Schiff base complexes and Cr (VI), revealing strategies to enhance their efficacy and exploring their potential for real-world applications.

RESULTS

Simulation studies on the adsorption of Cr (VI) ions

A structurally stable configuration of the TSA Schiff's base, characterized by minimal surface energy, was obtained using the Broyden-Fletcher-Goldfarb-Shanno (BFGS) optimization algorithm (Figure 1). The presence of heavy atomic species, such as Cr, induces dynamism in the pristine TSA Schiff's base, altering the atomic arrangement within the supercell and contributing to the overall dynamic stability of the system. This inherent dynamism makes the system an exceptional platform for the adsorption of heavy metals, making it an ideal candidate for in-depth adsorption studies. The total surface free energy of the TSA Schiff's base system is approximately −98.246 Ry. In contrast, the Cr (VI)-adsorbed TSA Schiff's base exhibits a total energy value of −979.762 Ry throughout the iterative optimization steps. This substantial increase in energy indicates that the adsorption of Cr (VI) ions imparts significantly enhanced dynamism—almost tenfold—to the TSA Schiff's base compared to its pristine state. This finding is consistent with previous studies on Cr(VI) adsorption.[12]

The configurations depicting the adsorption of the TSA Schiff's base molecule on $K_2Cr_2O_7$ in *S*-down, *S*-up, parallel, and vertical orientations are illustrated in Figure 1, along with their respective adsorption energies. The molecule exhibits weak adsorption on the surface for the S-down, S-up, and parallel orientations. Conversely, a negative adsorption energy was observed for the vertical orientation, indicating an unfavorable adsorption scenario. This implies that the molecule is more likely to desorb from the surface rather than adsorb in this orientation.

The density of states (DOS) has been graphed to observe the dynamic behavior of the TSA Schiff's base system (Figure 2) at both pre- and post-Cr (VI) ion adsorption. In both scenarios, overlapping states near the Fermi Level (indicated by a dotted vertical black line in Figure 2) are highlighted to elucidate the dynamic nature. This increase in total energy stems from the dispersion of Cr (VI) ions' atoms across the TSA Schiff's base surface, signifying complete delocalization of all Cr (VI) ions on the surface, unlike the localized nature of the TSA Schiff's base system. The pristine TSA Schiff's base system comprises solely localized states of C, S, and O atoms, resulting in lower total energy and lacking dynamic characteristics for Cr (VI) ion adsorption. Consequently, the emergence of delocalized surface states associated with Cr (VI) ions after adsorption, as opposed to the localized surface states of C, S, and O in the original TSA Schiff's base system, signifies a phase transformation. This transformation from localized to delocalized states renders the TSA Schiff's base system an effective surface for Cr (VI) ion adsorption. The delocalization of Cr (VI) ions over the TSA Schiff's base surface makes the system dynamic—approximately ten times more so compared to the pristine TSA Schiff's base system—for Cr (VI) ion adsorption studies, corroborating experimental findings.

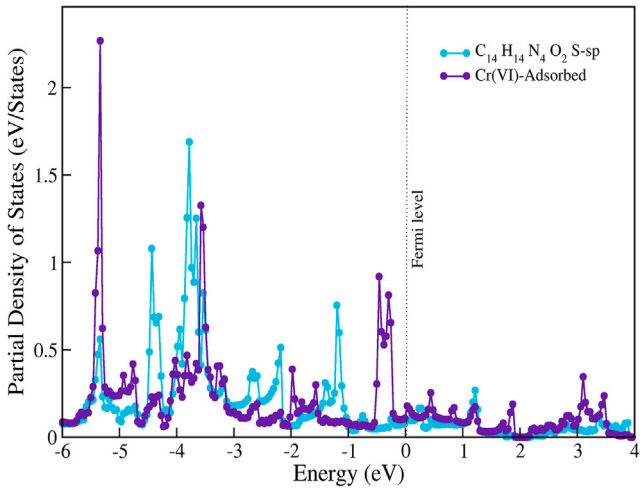

Figure 2. Simulated partial density of states (PDOS) plots for the TSA Schiff's base before Cr (VI) adsorption (in cyan) and after adsorption (in violet)
The dotted vertical black line is he Fermi level.

Material characterization

^{1}H NMR spectrum of the synthesized material

The Proton Nuclear Magnetic Resonance (^{1}H NMR) spectrum was recorded at a frequency of 400 MHz using deuterated dimethyl sulfoxide (DMSO-d_6) as the solvent. The spectrum exhibits chemical shifts and multiplicity patterns, which are characteristic of the functional groups present in the Schiff base. The multiplets in the region of 6.91 and 6.93 ppm corresponding to four protons indicate the presence of methine or methylene group in the benzene rings (Figure S1). The multiplets spanning between 7.29 and 7.41 ppm account for three protons, suggestive of the aromatic protons in the Schiff base. The singlets at 8.08 ppm, and 10.04 ppm indicate the presence of a single proton, closer to the electron-withdrawing hydroxyl groups owing to spatial conformation. The broader signal from 8.50 to 8.77 ppm corresponds to two protons of the secondary amine groups. A sharp peak at 11.63 ppm corresponds to a proton attached to the -C=N- carbon. Furthermore, the range from 11.89 to 12.08 ppm, exhibiting two broad signals, likely corresponds to two protons that are part of hydroxyl moieties.

Functional group characterization before and after adsorption studies

Before adsorption, the FTIR spectrum of the sorbent exhibits broad peaks with medium intensity, indicating -OH stretches of the weakly proton bonded hydrated adsorbent molecules at 3700 cm^{-1}, 3200 cm^{-1}, and the hydroxyl group of the salicylaldehyde functional group at 2703 cm^{-1}. A sharp peak at 3046 cm^{-1} represents the aromatic C-H stretch, while the imine group of the thiocarbohydrazide shows a medium-intensity stretching peak at 2950 cm^{-1}. The C=S stretching peak occurs at 2128 cm^{-1}, and the imine group displays an N-H bending stretch at 1626 cm^{-1}. In Figure 3A, it is observed that the intensities of the hydroxyl and amine groups in the sorbent molecule are slightly higher prior to adsorption. However, upon binding with Cr (VI) ions, the intensities of the spectral peaks for the bonded hydroxyl group at 3046 cm^{-1} and the amine stretch at 2950 cm^{-1} decrease. This reduction in intensity can be referred to the hydrogen bonding among the Cr (VI) ions and the active adsorption sites of the sorbent, which contain hydroxyl and amine functional groups. There are insignificant changes in the FTIR spectrum of post-adsorption which can be attributed to limited interaction strength, low surface coverage of the Cr (VI) ions on the adsorbent, and weak sensitivity due to structural integrity of the adsorbent.

Raman analysis before and after adsorption

The Raman spectra of as synthesized thiourea-salicylaldehyde complex, shown in Figure 3B divulges strong Raman peaks at 1577 and 1610 cm^{-1} and are attributed to the C=C stretching vibration of a benzene ring and C=N stretching vibration of thiourea-salicylaldehyde complex, respectively. The weak peaks at 1488 and 1455 cm^{-1} are attributed to NH deformation vibration and asymmetric C=C stretching vibration of the benzene ring, respectively. The weak C-H deformation vibrations occurred in the range of 1235–1250 cm^{-1}. The C-O stretching vibrations are found in the region of 1170–1190 cm^{-1}. The weak peak at 798 cm^{-1} is attributed to C-S stretching vibration. These Raman vibrational peaks are not affected due to Cr adsorption, as shown in Figure 3B.

X-Ray diffraction (XRD) analysis before and after adsorption

The XRD analyses were carried out in the angular range of $10° < 2\theta < 60°$ for the adsorbent both before and after chromium adsorption, as shown in Figure 3C. This approach aimed to provide a visual understanding of the structural changes occurring at the lattice level within the solid compounds. The XRD graph indicates a decrease in peak intensity and a right shift in peak positions following Cr (VI) adsorption.

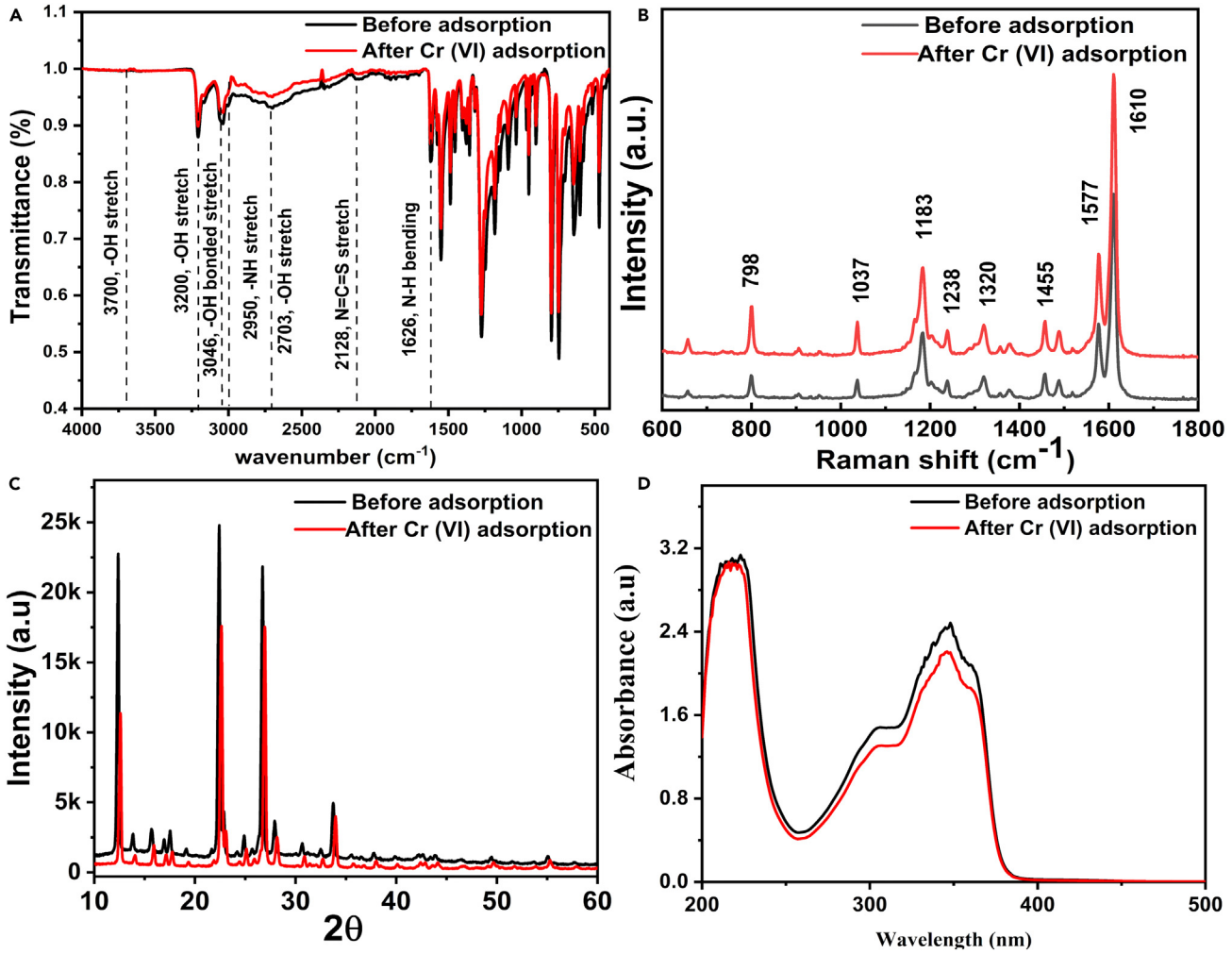

Figure 3. Characterization of Schiff base sorbent: FTIR, Raman, XRD, and UV-Vis analysis before and after Cr (VI) adsorption

Structural and functional characterization of the synthesized Schiff base (A) FTIR spectra of the sorbent before and after the adsorption of Cr (VI) ions, (B) Raman spectra comparison showing the changes in the spectrum before and after Cr (VI) adsorption, (C) XRD plot of the adsorbent before and after the adsorption of Cr (VI) ions and (D) UV-visible absorption maxima of the sorbent before and after the adsorption of Cr (VI) ions.

When heavy metal ions bind to the surface of an organic molecule, they can induce modifications in the molecular structure, potentially resulting in reduced crystallinity and diminished intensity of the XRD peak. This interaction can also disrupt the arrangement of organic molecules in the crystal lattice and a contraction of the unit cell, leading to weaker XRD peaks due to a decreased long-range order and right shift of XRD peak positions. Furthermore, the process of heavy metal adsorption has the capability to produce non-crystalline phases in the organic material, characterized by the absence of periodic crystalline patterns, thereby contributing to the observed decline in XRD peak intensity.

UV-visible spectroscopic analysis before and after adsorption

The formation of coordination complexes and the ensuing changes in the electronic structure are responsible for the hypochromic shift seen in the absorbance maxima of sorbent S6 at 346 nm, after the adsorption of Cr (VI) ions onto the molecular surface (Figure 3D). It is critical to consider the function of the dπ-pπ bonding to understand the UV-visible spectra in this investigation. When the Cr (VI) interacts with the Schiff base, a coordination bond is formed between the ion and the amine, hydroxyl functional groups of the Schiff base. The "dπ-pπ" bonding refers to the interaction between the Schiff base's p-orbitals (pπ) and the chromium ion's d-orbitals (dπ). This nature of bonding alters the electronic properties of the coordination complex, which impacts the adsorption of the metal ions. This distinctive bonding phenomenon has an intrinsic effect on the electronic cloud distribution within the complex, resulting in a consequential shift on electrons during the coordination. This redistribution of electrons impacts the absorption wavelengths of the complex, as compared to the pure Schiff base.[13,14]

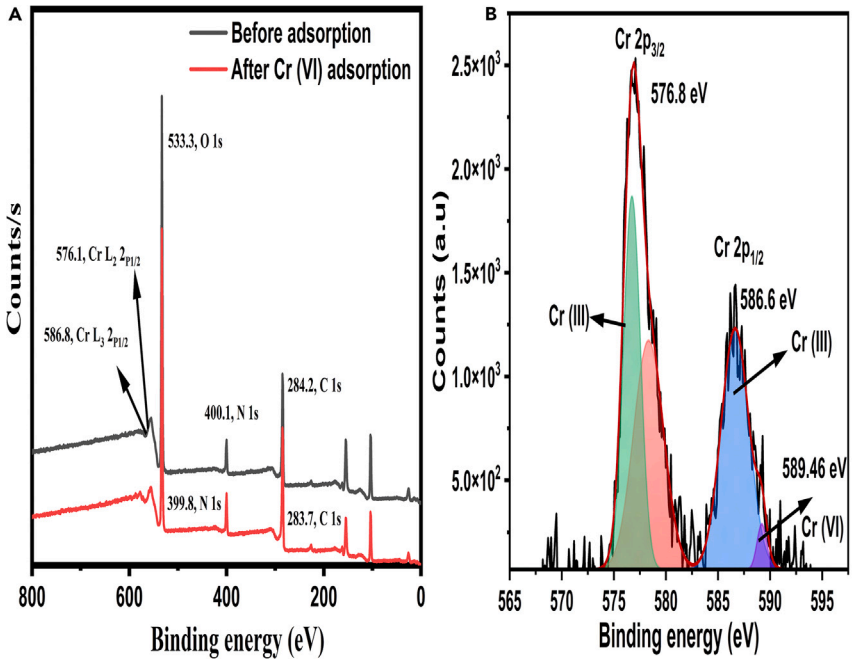

Figure 4. XPS analysis of Schiff base: survey spectra and high-resolution before and after Cr (VI) adsorption

XPS survey spectra of the Schiff base (A) before and after the adsorption of Cr^{6+} ions and (B) High-resolution peaks of Cr after adsorption.

X-Ray photoelectron spectroscopy before and after adsorption

The changes in the chemical composition resulting from the adsorption are evaluated using the XPS technique. As observed in Figure 4A, the XPS spectra of the Schiff base prior to adsorption reveal the core-level peaks corresponding to the constituent elements including carbon (283.7, C 1s), nitrogen (399.8, N 1s), and oxygen (533.3, O 1s). The binding energies of these elements were consistent with those reported in the literature for similar Schiff base compounds. The C 1s peak was mainly associated with carbon-nitrogen, C-N, and carbon-carbon, C-C, bonds present in the molecular structure of the Schiff base. The N 1s peak indicated the presence of amino and imine groups, indicating the characteristic functional groups of the Schiff base. The O1s peak was attributed to oxygen atoms within the carbonyl and hydroxyl moieties. Upon interaction with Cr (VI), considerable changes were detected in the XPS spectra of the Schiff base compound, as shown in Figure 4A. Notably, a shift in binding energies of the core-level peaks was observed, suggesting the development of new chemical bonds or interaction between the Schiff base and Cr (VI). The C 1s peak showed a slight shift toward higher binding energy (284.2, C 1s), indicating alterations in the carbon bonding environment. This could be attributed to the coordination of carbon atoms with Cr (VI) ions through the lone pairs of electrons present in the Schiff base structure. The N 1s peak exhibited a noticeable shift as well (400.1, N 1s), suggesting a coordination of nitrogen atoms with Cr (VI). This shift could be due to the donation of electron pairs from nitrogen atoms to Cr (VI) ions, forming coordination bonds. Moreover, the peak of the elemental O 1s displayed a decreased intensity, indicating modifications in the oxygen-containing functional groups of the Schiff base. Furthermore, supplementary peaks were detected at 576.1 (Cr L_2 $P_{1/2}$) and 586.8 (Cr L_3 $P_{1/2}$). These peaks aligned with the binding energies of distinct emission lines originating from the electron shells of the Cr (VI).[15,16]

The XPS spectra strongly suggest the interactions between the Schiff base and Cr (VI) ions. The peaks representing the core-level binding energies shift because of the coordination bond between the functional site of the Schiff base and Cr (VI). After Cr (VI) adsorption, the binding energies of 586.6 eV (Cr 2p1/2) and 576.8 eV (Cr 2p3/2) is attributed to Cr(III), while the peaks at 589.46 eV (Cr 2p3/2) correspond to Cr (VI) (Figure 4B). The XPS spectra after Cr (VI) adsorption indicated the reduction of Cr (VI) to Cr (III), with both species co-existing. After the reaction with Cr (VI), Cr (III) was found to be the predominant species of the adsorbed Cr ions on the adsorbent. This chelation effect brings about the rearrangement of the electronic density of the Schiff base, as a result of which, observe a minor shift in the binding energy peaks.

Morphological analysis using field emission scanning electron microscopy before and after adsorption

FE-SEM analysis has revealed a wide range of morphological diversity between the free Schiff base and the Schiff base- Cr (VI) complex. The micrographs exhibited distinct features, including particle size, shape, and surface texture which were attributed to the variations in the synthetic conditions and the effects of complexation. The particle size distribution of Schiff bases was calculated by measuring the width of individual crystals from FE-SEM images and observed to be ~3 μm, as shown in Figure 5. The results indicated that the synthesized material exhibited a flake-like structure. These variations in particle size can have significant implications for their applications, especially in catalysis and materials science. Surface texture analysis revealed the presence of irregularities, such as wrinkles and cracks on the surfaces of Schiff base

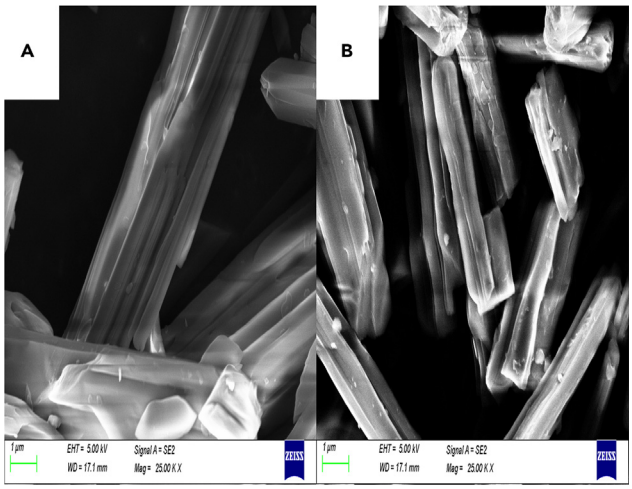

Figure 5. FE-SEM morphological analysis of Schiff base crystals: before and after Cr (VI) adsorption
FE-SEM morphological analysis of the Schiff base crystals, (A) before and (B) after Cr (VI) adsorption.

crystals. There are agglomerations in some Schiff base samples, leading to the formation of clusters or aggregates of particles. This phenomenon may be attributed to intermolecular forces.

Energy dispersive spectroscopy

The EDS analysis of the Schiff base compound prior to Cr (VI) adsorption revealed the elemental composition of the pristine crystal, as shown in Figure 6. The major elements identified in the EDS spectrum included nitrogen (N), hydrogen (H), carbon (C), and oxygen (O), which are consistent with the expected composition of the Schiff base. The absence of chromium peaks in the EDS spectrum before adsorption suggested that the crystal did not contain any detectable amounts of Cr (VI) prior to exposure to the adsorbate. This indicates the purity of the Schiff base crystal and the absence of any intrinsic chromium impurities. Following the exposure of the Schiff base compound to Cr (VI) ions, the EDS analysis was repeated to assess any changes in the elemental composition of the crystal. The presence of new peaks corresponding to chromium (Cr) in the post-adsorption EDS spectrum indicated the efficient adsorption of Cr (VI) ions onto the Schiff base crystal, as shown in Figure 6B. The quantitative analysis of the EDS data indicated the incorporation of chromium into the crystal lattice, with a significant increase in chromium content compared to the initial state. This demonstrates the efficient adsorption capability of the Schiff base crystal for Cr (VI) ions.[17]

Dynamic light scattering for particle size measurements

By detecting the variations in scattered light caused by Brownian motion, dynamic light scattering (DLS), a powerful method, may be used to analyze the size distribution of particles or molecules in a solution. The behavior and size distribution of particles and molecules that interact with the solution may alter the DLS plot, as seen in Figure 3. The observed shift in the DLS plot from 21 nm to 43 nm for the adsorption of Cr(VI) can be ascribed to the adsorption of Cr ions onto the particles or sorbent molecules present in the solution. Due to their propensity to bond to surfaces, chromium ions could be adsorbed onto the surfaces of the particles or sorbent molecules being studied. Several outcomes are conceivable when chromium binds to these particles or molecules. One hypothesis is that the Cr (VI) ions can really surround the particles or molecules in new layers, increasing their size and shifting the DLS plot toward higher sizes.[18,19] The particles or molecules may also aggregate or agglomerate because of the adsorbed chromium species, resulting in the development of bigger clusters that contribute to the increased size seen in the supplementary section of the MS (Figure S2).

Surface area and pore volume analyses

The surface area results (Figure 7A) show that the Schiff base crystals have a specific surface area (SSA) of 6.0569 $m^2 g^{-1}$, and a total pore volume of 1.3916 cm^3/g. The pore size distribution of the prepared Schiff base is shown in Figure 7B. A few peaks were detected, with the sharpest peak occurring at a pore diameter between 1.49 and 3.15 nm and the mean pore diameter of 12.817 nm. The results indicate a mesoporous structure of Schiff base crystals according to the IUPAC classification.[20] The SSA of Schiff base crystals decreased to 4.0199 $m^2 g^{-1}$ after Cr (VI) adsorption. This decrease is due to the decrease in the active site available for N_2 adsorption which is already occupied by the Cr (VI) ion.

Optimization of the adsorption parameters

Impact of pH and point of zero charge

To investigate the interaction mechanism between Cr (VI) and the adsorbent, the electrokinetic properties of the adsorbent were assessed. Figure 8A illustrates the experimental data using the salt addition approach, presenting plots of initial pH versus change in pH. The point

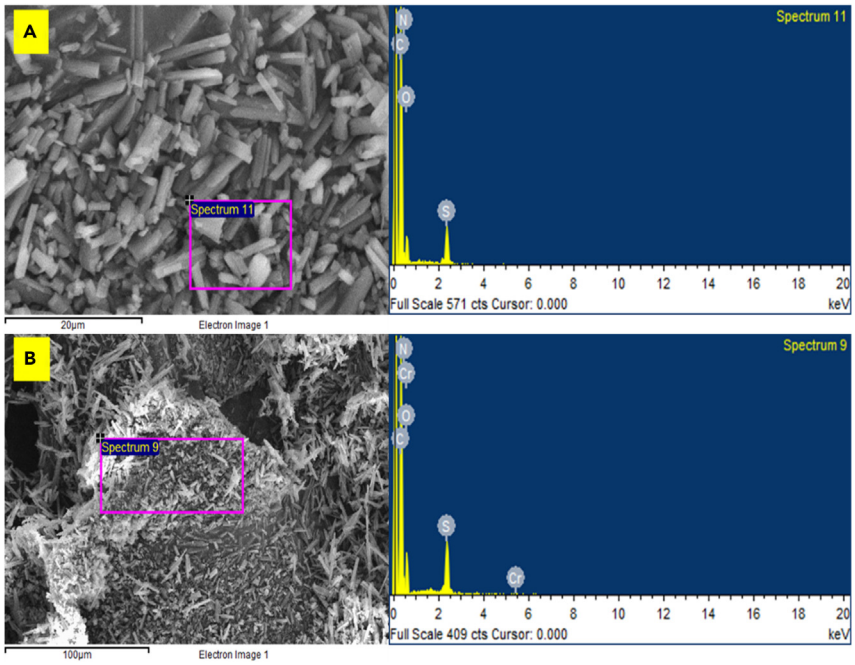

Figure 6. EDS analysis of Schiff base crystals: elemental composition before and after Cr (VI) adsorption

Illustration of Energy Dispersive Spectroscopic (EDS) analysis of Schiff base crystals (A) before and (B) after the adsorption of Cr (VI).

of zero charge (pH_{PZC}) was determined using sodium nitrate of ionic strength 0.1 M. Across the pH range of 2–10, the pH_{PZC} was 5.26 at room temperature (Figure 8A). The pH of a solution has a crucial impact on governing the adsorption process. As depicted in Figure 8B, the adsorption of Cr (VI) ions using the Schiff base is contingent upon pH, with the removal efficiency diminishing as the pH is elevated from 3 to 10. In Figure 8B, a graphical representation is provided, illustrating the absorptivity and treatment efficiency of Cr (VI) across various pH levels.

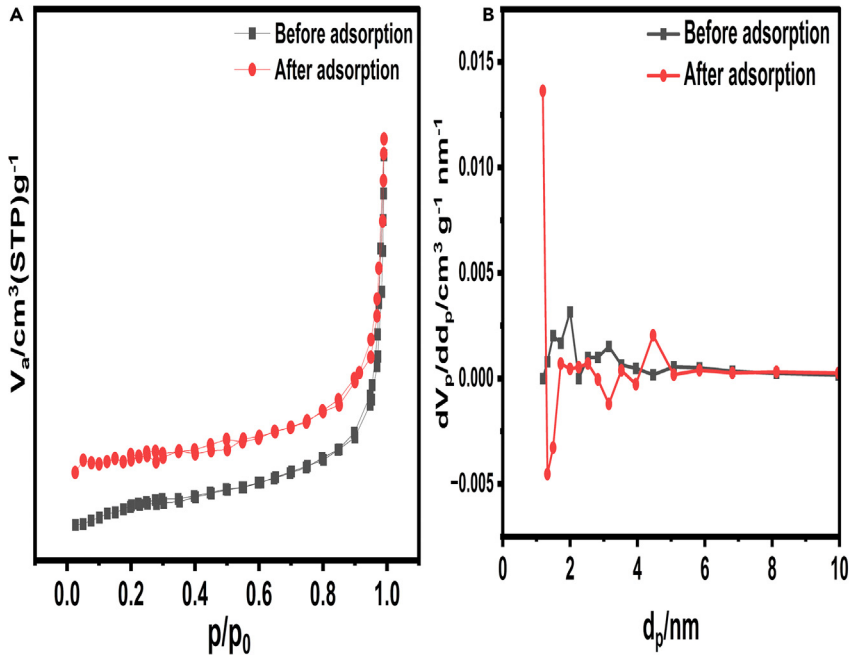

Figure 7. BET analysis of Schiff base: SSA and pore size distribution before and after Cr (VI) adsorption

BET results, (A) SSA of the Schiff base before and after Cr (VI) adsorption and (B) Pore size distribution of the Schiff base before and after Cr (VI) adsorption.

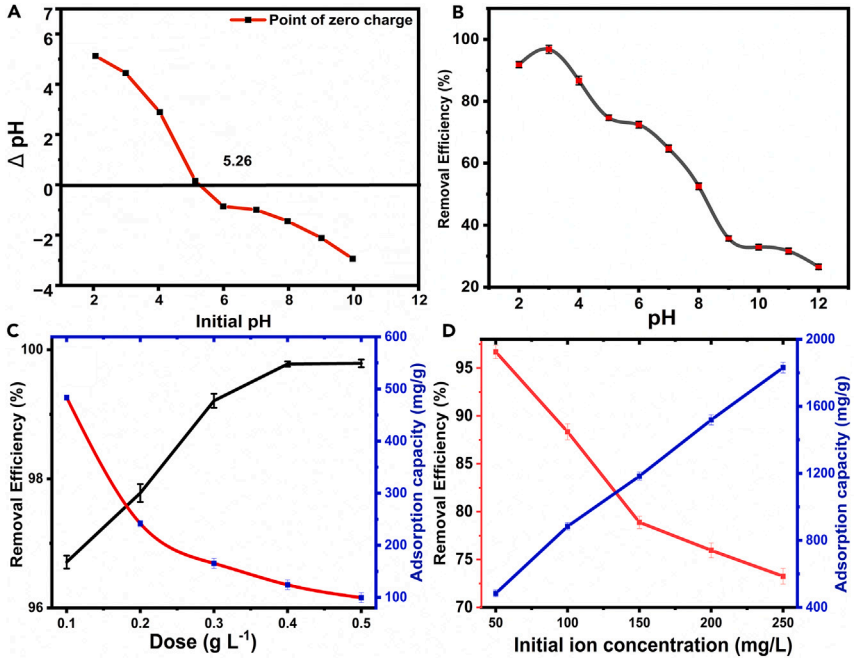

Figure 8. Influence of adsorption conditions on Cr (VI) uptake: pHPZC, pH, dose, and initial ion concentration

Effect of adsorption conditions on Cr (VI) adsorption (A) pH_{PZC}, (B) impact of pH (C) impact of dose and (D) impact of initial ion concentration.

Impact of dose

The correlation between the amount of adsorbent and Cr (VI) may be ascribed to the presence of binding sites and the expanded surface area provided by the sorbent, as agreed with previous studies.[21] To study the effect of adsorbent dosage on the scavenge of Cr (VI), experiments were conducted with varying doses ranging from 0.1 to 0.5 g/L. The lowest removal efficiencies, at 0.1 g/L dosage, were measured at 96.8% and these values increased to maximum levels of 99.52% for doses of 0.5 g/L (Figure 8C). This suggests that initially, there is a rapid uptake of Cr (VI) on the Schiff base due to the abundance of unoccupied adsorption sites for binding. As the adsorbent dosage increases, the saturation of the Schiff binding sites for Cr (VI) sorption occurs, leading to a pronounced reduction in removal efficiency. Beyond a dosage of 0.5 g/L, increasing the concentration of Schiff has minimal impact on removal efficiency, as an equilibrium or saturation point is reached between the Cr (VI) ions and the adsorbent. At this stage, adsorption becomes challenging due to the electrostatic repulsive forces between the Cr (VI) ions and the surface of the Schiff.

Effect of initial Cr (VI) ions concentration

The impact of Cr (VI) initial concentration on the removal of Cr (VI) from water was investigated under specific experimental program: pH set at 3, adsorbent dosage of 0.1 g/L, and a residence time of 180 min. In Figure 8D, the results of the experimental study regarding the influence of Cr (VI) ion concentration (ranging from 0.05 to 0.25 g L^{-1}) are presented. As Cr (VI) initial concentration increased, the adsorptivity of Schiff base also increases. This behavior is attributed to the fact that at lower Cr (VI) concentrations, there are ample available adsorption sites, facilitating rapid adsorption. However, when the Cr (VI) concentration >0.25 g/L, the maximum adsorptivity is reached. At this point, a considerable number of Cr (VI) ions compete for the limited surface adsorption sites on the Schiff base, leading to a reduction in the adsorptivity of the ions. However, the adsorption tendency increased at higher initial concentrations while the removal percentage reduced.[22] This is because, with a fixed adsorbent dose, a higher initial concentration leads to a greater likelihood of saturating the interior active sites. As the Cr (VI) concentration rises, all available active sites on the adsorbent become linked to the metal ions, resulting in an increase in adsorption capacity.

Kinetic studies

The residence time between a sorbent and an adsorbate is considerably affect the adsorption capacity. Figure 9 show that the adsorption rate of Cr (VI) onto TSA is fast during the first 4 h of contact followed by slower rate of uptake (4–6 h) and finally the equilibrium occur after 6 h. However, the same observation was recorded for all the Cr (VI) initial concentrations (0.05–0.25 g/L) owning to the uniform structure of the developed TSA. The corresponding adsorption capacities of TSA toward Cr (VI) at concentrations 0.05, 0.1, 0.15, 0.2 and 0.25 g/L were 483.5, 883.5, 1183.5, 1519.3 and 1831.3 mg/g, respectively. The fast rate of Cr (VI) uptake onto the TSA is expected owning to the abundance of free active sites of the TSA at the beginning of the adsorption process and the diffusion of the metal ions in the solution is high owning to

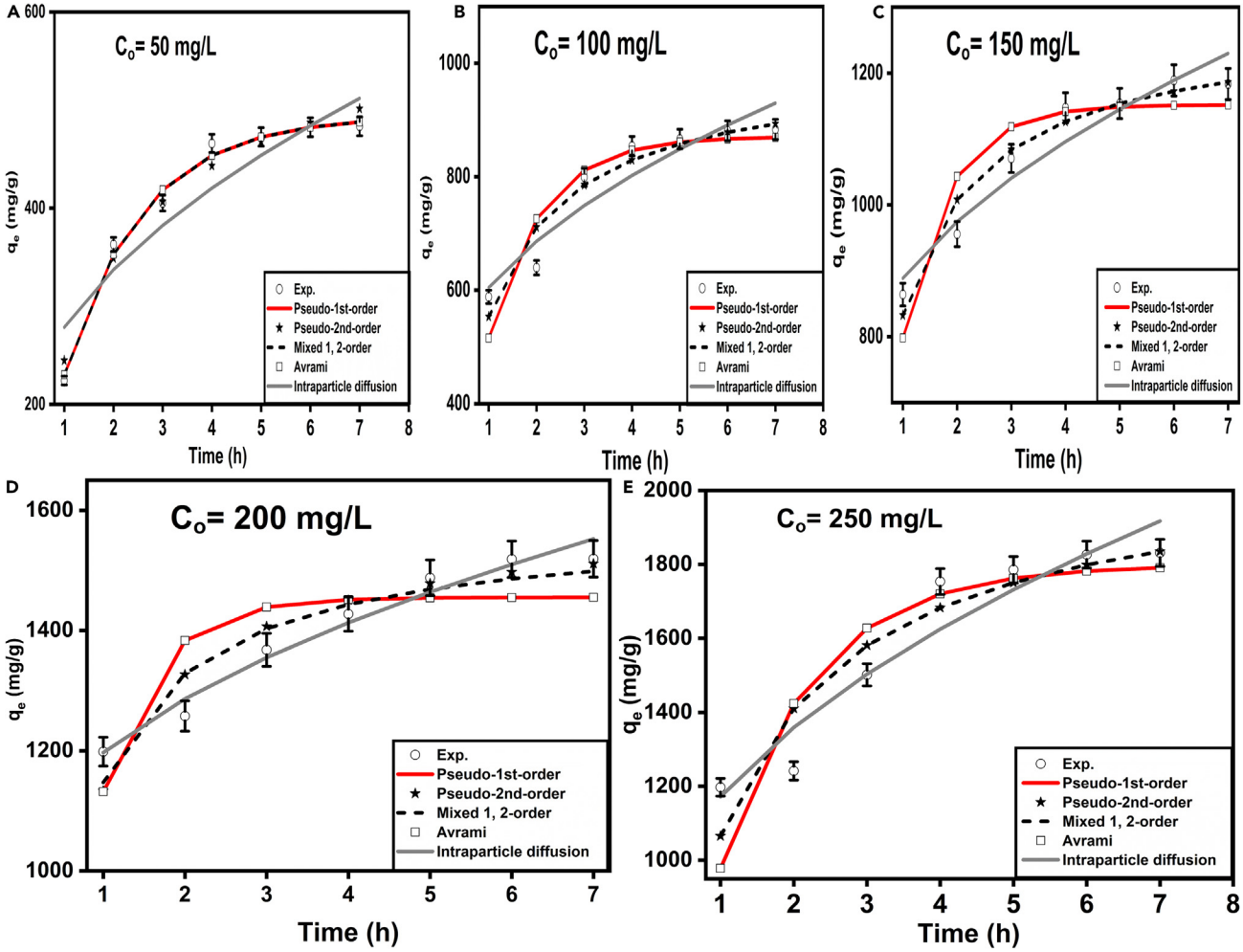

Figure 9. Model fitting of Cr (VI) adsorption on TSA: comparison of kinetic models at varying initial concentrations

Matching of the experimental data to Pseudo-1st-order, Pseudo-2nd-order, Avrami, mixed 1st & 2nd-orders, and IPD models for the arrays results of the Cr (VI) adsorption onto TSA at initial concentrations of 0.05 (A), 0.1 (B), 0.15 (C), 0.2 (D), and 0.25 (E) g/L (without considering the zero value as starting point.

the concentration gradient between the Cr (VI) in the solution and the adsorbent surface while the slower rate of adsorption in the second stage until the equilibrium is occur could be owned to the resistance toward the diffusion of the metals ions into the outer and inners surface of TSA where this concentration gradient is decreased. To study the kinetic of Cr (VI) adsorption onto TSA, five adsorption kinetic models were studied (Figure 9).

The kinetic parameters are presented in Table 1. Out of all models, Avrami model is the best to control the adsorption system under investigation where the values of experimental adsorption capacities (483.5, 883.5, 1183.5, 1519.3, and 1831.3 mg/g) are close to the predicted one (493.9, 870.8, 1151.9, 1454.99 and 1798.0 mg/g which are corresponding to Cr (VI) initial concentrations 0.05, 0.1, 0.15, 0.2 and 0.25 g/L, respectively) in addition to the higher correlation coefficient especially at initial concentration 50 mg/L (R^2 0.99). By comparing the correlation coefficients at higher concentrations, it can be noticed that with increasing the initial concentration of the metal ions, the R^2 decreased, which means that this model can be used to match the data accurately at lower concentrations where increasing the initial concentration of Cr (VI) from 0.05 to 0.25 g/L decreases the correlation coefficient from 0.99 to 0.78. This is agreed with the actual circumstances of wastewater where the Cr (VI) can be detected. Although the mixed 1 and 2-order model yield high R^2, However, the predicted values of adsorption capacites are 493.9, 995.1, 1276.8, 1579.0 and 2084.8 mg/g which are corresponding to Cr (VI) initial concentrations 0.05, 0.1, 0.15, 0.2 and 0.25 g/L are much higher than the calculated one with special focus at higher inital cncentrations. This is also agreed with Avrami where both models can fitt the data accurately at $C_o \leq 0.05$ g/L.

The results of *n* values suggest also that the adsorption system under study is Cr(VI) initial concentration-dependenant process The traditional Pseudo-1st-order and Pseudo-2nd-order don't fit the data well. The predicted values of both models are much higher than the expermental one even the correlation coefficent (R^2) show high values (0.97) in lower concentrations (Table 2). On the other hands, the IPD model is

Table 1. Factors of the kinetic models for the adsorption of Cr (VI) onto TSA

Model	Co [g/L]	0.05	0.1	0.15	0.2	0.25
	q_{exp} [mg/g]	483.5	883.5	1183.5	1519.3	1831.3
Pseudo-1st-order	K_1 [min^{-1}]	0.001	0.897	1.180	1.5051	0.785
	q_e [mg/g]	607.6	870.8	1151.9	1454.9	1798.0
	R^2 [-]	0.97	0.85	0.82	0.64	0.78
Pseudo-2nd-order	K_2 [g/mg.min]	0.001	0.001	0.001	0.0015	0.0005
	q_e [mg/g]	607.6	995.1	1276.4	1600	2086.0
	R^2 [-]	0.97	0.92	0.95	0.88	0.87
Mixed 1 and 2-order model	K [$mg/g.min^{-1}$]	0.627	0.001	0.0008	0.0007	0.0007
	q_e [mg/g]	493.9	995.1	1276.8	1579.0	2084.8
	f_2 [-]	0	0.999	0.999	0.999	0.999
	R^2 [-]	0.99	0.92	0.95	0.89	0.87
Avrami	q_e [mg/g]	493.9	870.8	1151.9	1454.9	1798.0
	k_{av} [min^{-1}]	0.814	0.974	1.1174	0.808	2.17
	n_{av} [-]	0.769	0.921	1.0561	1.862	0.362
	R^2 [-]	0.99	0.85	0.82	0.64	0.78
IPD	k_{ip} [$mg/g.min^{1/2}$]	141.9	197.7	207.3	215.9	453.1
	c_{ip} [mg/g]	136.6	406.7	681.3	981.1	718.7
	R^2 [-]	0.86	0.89	0.93	0.97	0.91

not approprate for the adsorption system under study where the calculated data don't match with the expermental one (Figure 9) showing that the adsorption of the metal ions onto the TSA is not manged by the diffusion into the adsorbent.

The above-mentioned models were also fitted to the expermental data of Cr (VI) adsorption onto TSA considering zero values of Cr (VI) initial concentrations, and it was found that Pseudo-1st-order, Pseudo-2nd-order, mixed 1st and 2nd-order and Avrami models can accuratly describe the expermental data (Figure S1) and the values of R^2 are high (Table 1) under all initial concentraions of Cr (VI) while the IPD model is stilll not appropriate for the adsorption system under study.

Adsorption modeling

The adsorption isotherms are significant in exploring the mechanism and adsorption affinity of TSA toward Cr (VI). Subsequently, eleven models; Freundlich, Langmuir, Redlich-Peterson, Temkin, Langmuir-Freundlich, Sips, Dubinin–Radushkevich, Toth, Khan, Baudu and Fritz-Schlunder models were implemented to match the experimental data of Cr (VI) adsorption onto TSA at room temperature based on the non-linear forms of these models as seen in Figure 10 and Table 2.

Figure 10B shows that the Freundlich model is the predominant adsorption models that fit the experimental data as well as R^2 = 0.98 (Table 2). This model indicates the surface heterogeneity of TSA and the exponential distribution and energy of the active sites onto TSA. The value of 1/n (0.394) shows that the type of isotherm is favorable.[23] On the other hand, Dubinin–Radushkevich, Temkin and Langmuir models (Figure 10B) couldn't describe the experimental data as well as their correlation coefficients are low (0.73, 0.89, and 0.87, respectively). Redlich-Peterson (Figure 10C), Sips (Figure 10D), Langmuir-Freundlich (Figure 10D), and Toth (Figure 10E) are not appropriate to explore the Cr (VI) @TSA adsorption systems, despite of their high corresponding correlation coefficients (R^2 = 0.98, 0.98, 0.97, and 0.98, respectively) owning to that the predicted maximum adsorption capacities are much higher than the experimental one. Also, Khan (Figure 10E), Baudu and Fritz-Schlunder models (Figure 10A) are also not efficient in describing the Cr (VI)@TSA adsorption system, despite the high yielded correlation coefficients (0.98, 0.98, and 0.98) where the calculated values of maximum adsorption capacities using these models are much less than that of experimental one (Table 2).

In conclusion, the strong alignment of the experimental results with the Freundlich model indicates that the adsorption of Cr(VI) onto the TSA base exhibits characteristics of heterogeneous surface adsorption. This suggests the presence of both monolayer and multilayer adsorption mechanisms for Cr(VI), consistent with the kinetic findings.

Comparison study

To prove the practicality of the newly developed nanocomposite as a highly effective adsorbent for removing Cr (VI), the adsorption capacity of the TSA nanocomposite was compared to that of other materials and nanocomposites mentioned in previous studies that employed similar batch adsorption experiments (Table 3). Based on the comparison, the nanocomposite discussed in this research has the potential to be used as an adsorbent for the extraction of Cr (VI) from wastewater.

Table 2. The parameters of the adsorption models for Cr (VI) adsorption onto TSA

Model	Parameter	Value	Parameter	Value
Langmuir	q_{max} [mg/g]	2061.6	R^2 [-]	0.87
	K_L	0.064		
Freundlich	1/n	0.394	R^2 [-]	0.98
	K_F [L/mg]	333.3		
Temkin	BT	7.44	R^2 [-]	0.89
	AT	1.86		
Dubinin–Radushkevich	q_m [mg/g]	1841.4	R^2 [-]	0.73
	Kad	0.002		
Langmuir-Freundlich	q_{MLF} [mg/g]	43493.3	M_{LF}	0.405
	K_{LF}	5.9E-06	R^2 [-]	0.97
Sips	q_m [mg/g]	11.8 E05	1/n	0.395
	K_s	0.0003	R^2 [-]	0.98
Redlich-Peterson	K_R	59.7E04	β	0.611
	a_R	1758.0	R^2 [-]	0.98
Toth	K_t	21.9E05	z	0.605
	a_T	10866.8	R^2 [-]	0.98
Khan	q_m [mg/g]	20.8	a_K	0.605
	b_K	1124.0	R^2 [-]	0.98
Baudu	q_m [mg/g]	333.3	x	0.394
	b_0	41764.8	y	0.080
			R^2 [-]	0.98
Fritz-Schlunder	q_{mFSS} [mg/g]	44.7	m_1	0.394
	K_1	7.62	m_2	0
	K_2	0.022	R^2 [-]	0.98

Regeneration studies

The reusability of the adsorbent in the decontamination of Cr (VI) from simulated wastewater was assessed, and desorption experiments were conducted, employing three different regenerants (0.1M HCl, 0.1 M HNO_3, and 0.1 M NaOH) at room temperature for 180 min (Figure 11). The adsorbent was successfully regenerated for up to seven cycles for the removal of Cr (VI) from synthetic water. The decrease in reusability can be attributed to the destruction of functional groups and active sites while using regenerates. It can be seen that the acidic reagents are better than the alkaline ones. The best results were achieved with 0.1 HCl, where the efficiency of Cr(VI) removal gradually decreased from 93.3% in the first cycle to 86.68% by the third cycle, and significantly dropped to 59.23% by the sixth cycle. Similarly, 0.1 HNO3 showed a decrease in removal efficiency from 74.72% in the first cycle to 54.36% by the third cycle. The lowest removal efficiency was observed with 0.1 NaOH, where the removal percentage declined from 58.42% in the first cycle to 11.06% by the sixth cycle. Future studies should investigate other reagents to improve performance. These results highlight the adsorbent's significant ability to effectively release and re-capture Cr(VI), suggesting its promising potential for industrial applications in removing chromium from wastewater streams.

DISCUSSION

This study confirmed the synthesis of Schiff base produced from thio-carbohydrazide and salicylaldehyde and was characterized by different techniques FTIR, UV, XRD, SEM-EDX, Raman, XPS, 1H NMR, and BET, and its adsorption behavior as an adsorbent for Cr (VI) removal. The effect of dosage, pH, and Initial ion concentration were examined using batch mode studies. The optimum conditions for better performance were pH 3, 0.1 g/L of dosage, and an ion concentration of 50 mg/L. It shows remarkable removal efficiency greater than 97%. The synthesized material exhibits a point of zero charges near pH 5.26, and the maximum adsorption was seen at pH 3. Chromium (VI) ions can manifest in distinct anionic forms, such as $HCr_2O_7^-$, $Cr_2O_7^{2-}$, $HCrO_4^-$, and CrO_4^{2-}, depending upon the solution's pH and concentration. At highly acidic pH levels below 2, Cr (VI) predominantly presents in the H_2CrO_4 form. In the pH range between 2.0 and 6.0, it is commonly encountered in the forms of $HCr_2O_7^-$, and $Cr_2O_7^{2-}$. As the pH rises above 7, it predominantly takes on the CrO_4^{2-} form. Nevertheless, it's worth noting that at pH levels below 3.0, a reduction in adsorption capacity is evident due to the presence of Cr in the form of H_2CrO_4. At these lower pH values, a pronounced competition arises between H_2CrO_4 and protons for binding sites on the adsorbent. Under acidic conditions, functional groups may become protonated, leading to robust electrostatic interactions between the adsorbent and the $Cr_2O_7^{-2}$ ion. Conversely, within the pH

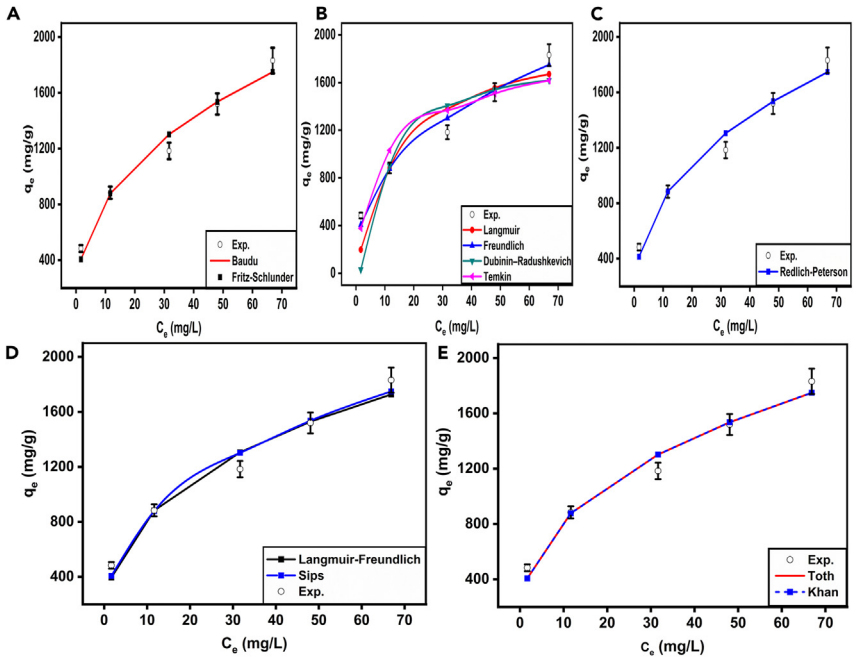

Figure 10. Adsorption isotherm fitting for Cr (VI) on TSA: comparative analysis of multiple models

Fitting the expermental data of the Cr (VI) adsorption onto TSA using Fritz-Schlunder and Baudu (A), Langmuir, Freundlich, Dubinin–Radushkevich and Temkin (B), Redlich-Peterson (C), Sips and Langmuir-Freundlich (D), Toth and Khan (E).

range of 5.0–7.0, the primary form of Cr is CrO_4^{2-}. In this pH range, an abundance of OH- ions in the Cr solution competes with chromate (CrO_4^{2-}) ions for the adsorption onto the surface of the adsorbent, with OH^- ions typically prevailing. Consequently, as the pH increases, the adsorption capacity of Cr (VI) diminishes. The adsorption capacity of Schiff base also exhibits a decline as the pH increases, reaching its maximum adsorption capacity at pH 3.0 and then significantly decreasing at pH 7. These observations align with findings from prior research.[30]

Table 3. Comparative analysis of Cr (VI) adsorption with previously reported adsorbents

Adsorbent	C_o (mg/L)	q_e (mg/g)/ Percentage removal	Dosage (g/L)	pH	References
TSA	50–250	1831.3 (>97%)	0.1	3	This work
MOF-5	50	78.12	1	2	Babapour et al.[24]
MOF BUC-17	40	121	0.25	4	Guo et al.[25]
Fe_3O_4@MIL-100	10–100	18	0.004	2	Yang et al.[26]
ZIF-8	2.5	0.25	0.02	7	Niknam Shahrak et al.[27]
Mn-UiO-66	10	32.77	0.2	–	Yang et al.[28]
ZnO-GO	5–25	3.69 (96%)	2	8.02	Singh et al.[29]
CaO-GO	10–50	38.04	1	3	Singh et al.[30]
UiO-66-NH_2	5	32.36	1	6.5	Wu et al.[31]
chitosan schiff base & $MnFe_2O_4$ nanoparticles@biochar	20–100	125.34	0.01	2	Yan et al.[32]
Chitosan phenyl-1H-pyrazolo[3,4-b] quinoxaline Schiff base	5–1000	147.6	0.150	6	Elhag et al.[33]
Graphene oxide @Schiff base	20–100	76.92	0.03	3	Anush et al.[34]
Nitrogen doping hydrothermal carbon with Schiff base structure	50–600	349.6	1	2	Wei et al.[35]
Mesoporous silica with Schiff base	50	0.046	4	2	Boorboor and Behzad[36]

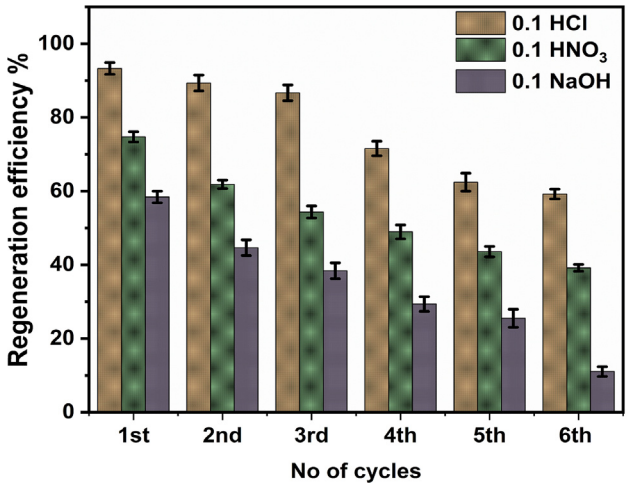

Figure 11. Reusability of the adsorbent using three different reagents

In the kinetics studies, the Avrami model best describes the adsorption process. The goodness-of-fit achieved by Cr(VI) adsorption into the Avrami model can be attributed to the model's flexibility in accounting for complex adsorption routes that consider both chemical and physical interactions between Cr(VI) and the adsorbent. As shown in Table 1, the value of k_{av}, simulated from the Avrami model, increases with the initial concentration of Cr(VI). This indicates that the adsorption equilibrium is reached faster at higher concentrations, likely due to the greater concentration gradient between the Cr ions in the solution and those at the adsorbent surface, which enhances the mass transfer process. The increase in k_{av} with higher initial concentrations suggests that both physisorption and chemisorption are involved in the adsorption mechanism. Meanwhile, n_{av} is a fractional number that refers to possible changes in the adsorption mechanism during the process. If $n_{av} = 1$, it signifies a uniform adsorption process. If $n_{av} = 2$, it may indicate a one-dimensional growth of adsorption sites after uniform adsorption.[37] The magnitude of the Avrami exponent varies with the initial Cr(VI) concentration, ranging from 0.769 to 1.862 for concentrations from 0.05 to 0.2 mg/L, indicating that Cr(VI) adsorption involves multiple routes.[38] At a higher Cr(VI) concentration (0.25 mg/L), the value of n_{av} drops to 0.362, which may be attributed to the fact that, at higher values of n, the diffusion of Cr ions is faster than the mass transfer process.[39] Additionally, regeneration experiments were also conducted to confirm its reusability and effectiveness. The capability of regeneration demonstrated through the successful reuse of the adsorbent for up to three cycles, with a removal capacity exceeding 86.68%, adds a novel dimension to this study. This unprecedented reusability can be attributed to the preservation of active sites in the adsorption cavities of the Schiff base complexes, thereby making Schiff bases a revolutionary candidate for sustainable and cost-effective remediation of industrial wastewater.

Conclusions

In conclusion, this study demonstrates the exceptional potential of the Schiff base derived from thiocarbohydrazide and salicylaldehyde as an effective adsorbent for Cr(VI) removal from industrial wastewater. The effect of dosage concentration on the adsorption rate was evaluated, and eleven different adsorption isotherms were employed to gain a comprehensive understanding of the adsorption affinity of the Schiff base adsorbent toward Cr(VI). The results suggests that the Freundlich model best describes the Cr(VI) adsorption on the Schiff base ($R^2 = 0.98$). Additionally, the kinetics of the adsorption system indicate that the Avrami model provides the best fit for the experimental data ($R^2 = 0.99$).

Simultaneously, the experimental outcomes are reinforced by theoretical density functional theory simulations. These simulations reveal that the TSA Schiff's base system exhibits an enhanced dynamic nature, particularly notable for heavy metal adsorption studies, attributed to the presence of delocalized surface states. The notable capacity of the composite to adsorb and desorb Cr (VI) further underscores the potential utility representing a paradigm shift in addressing heavy metal pollution in wastewater treatment. The present study not only advances our understanding of the vast potential of the Schiff bases as sorbents but also opens new avenues for practical applications emphasizing the transformative impact of Schiff base complexes in environmental remediation.

Limitations of the study

The limitations of this work include the need to assess the cytotoxicity of the developed composite, conduct a cost analysis for large-scale applications, and investigate the selectivity of the adsorbent toward Cr(VI) in the presence of other emerging contaminants in real wastewater samples. Additionally, it is strongly recommended to search for alternative reagents, particularly those that are environmentally friendly and sustainable.

RESOURCE AVAILABILITY

Lead contact

Requests for further information and resources should be directed to the lead contact, author: Praveen C Ramamurthy (onegroupb203@gmail.com).

Materials availability

This study did not generate new materials.

Data and code availability

- NMR spectrum of the sorbent with aromatic region is presented in Figure S1 while DLS plots of the sorbent before and after adsorption of Cr^{6+} ions is presented in Figure S2 (are available in the accompanying supplementary dataset).
- This study does not report original new code.
- Any additional information required to reanalyze the data reported in this article is available from the lead contact upon request.

ACKNOWLEDGMENTS

Dr. Simranjeet Singh would like to acknowledge DBT HRD Project & Management Unit, Regional Centre for Biotechnology, NCR Biotech Science Cluster, Faridabad, Haryana, for Research Associateship (DBT-RA), fellowship under award letter No DBT-RA/2022/July/N/2044 dated January 12, 2023. The authors wish to express their gratitude to the Ministry of Education (MoE) for their support under the grant MoE-STARS/STARS-2/2023–0714, dated September 26, 2023. SKB would like to acknowledge UCG, Govt. of India for Dr. D. S. Kothari Postdoctoral Fellowship under award No.F.4–2/2006 (BSR)/PH/20–21/0108, dated 14/09/2021.

AUTHOR CONTRIBUTIONS

Simranjeet Singh: Conceptualization, data curation, formal analysis, investigation, methodology, and original draft writing - review and editing. Shweta Shekar, Nadeem A Khan, Joginder Singh, and Nabila Shehata: Formal analysis, investigation, methodology, and writing, review and editing. S.K Behera: Simulation studies and respective analysis. Praveen C. Ramamurthy: Resources, project guidance, supervision, validation, and writing, review and editing.

DECLARATION OF INTERESTS

The authors declare no conflicting interests.

STAR★METHODS

Detailed methods are provided in the online version of this paper and include the following:

- KEY RESOURCES TABLE
- METHOD DETAILS
  - Chemicals and solvents
  - Material synthesis
  - Material characterization
  - Kinetics & isotherms
  - Adsorption modelling
  - Density functional theory studies
- QUANTIFICATION AND STATISTICAL ANALYSIS

SUPPLEMENTAL INFORMATION

Supplemental information can be found online at https://doi.org/10.1016/j.isci.2024.110925.

Received: May 12, 2024
Revised: August 27, 2024
Accepted: September 9, 2024
Published: September 13, 2024

REFERENCES

1. Singh, S., Naik, T.S.S.K., Thamaraiselvan, C., Behera, S.K., N, P., Nath, B., Dwivedi, P., Singh, J., and Ramamurthy, P.C. (2023). Applicability of new sustainable and efficient green metal-based nanoparticles for removal of Cr(VI): Adsorption anti-microbial, and DFT studies. Environ. Pollut. *320*, 121105. https://doi.org/10.1016/J.ENVPOL.2023.121105.
2. Mishra, S., and Bharagava, R.N. (2016). Toxic and genotoxic effects of hexavalent chromium in environment and its bioremediation strategies. J. Environ. Sci. Health C Environ. Carcinog. Ecotoxicol. Rev. *34*, 1–32. https://doi.org/10.1080/10590501.2015.1096883.
3. Vinuth, M., Naik, H.B., sekhar, K.C., Manjanna, J., and Vinoda, B.M. (2015). Environmental Remediation of Hexavalent Chromium in Aqueous Medium Using Fe(II)-Montmorillonite as Reductant. Procedia Earth Planet. Sci. *11*, 275–283. https://doi.org/10.1016/j.proeps.2015.06.036.
4. Wang, X.S., Chen, L.F., Li, F.Y., Chen, K.L., Wan, W.Y., and Tang, Y.J. (2010). Removal of Cr (VI) with wheat-residue derived black carbon: Reaction mechanism and adsorption performance. J. Hazard Mater. *175*, 816–822. https://doi.org/10.1016/J.JHAZMAT.2009.10.082.
5. Balakrishna Prabhu, K., Saidutta, M.B., and Srinivas Kini, M. (2017). Adsorption of hexavalent chromium from aqueous medium using a new Schiff base Chitosan Derivative. Int. J. Appl. Eng. Res. *12*, 4072–4082.
6. Sugashini, S., and Begum, K.M.M.S. (2013). Optimization using central composite design (CCD) for the biosorption of Cr(VI) ions by cross linked chitosan carbonized rice husk (CCACR). Clean Technol. Environ. Policy *15*,

293–302. https://doi.org/10.1007/s10098-012-0512-3.
7. Alluhaybi, A.A., Alharbi, A., Hameed, A.M., Gouda, A.A., Hassen, F.S., El-Gendy, H.S., Atia, B.M., Salem, A.R., Gado, M.A., Ene, A., et al. (2022). A Novel Triazole Schiff Base Derivatives for Remediation of Chromium Contamination from Tannery Waste Water. Molecules *27*, 5087. https://doi.org/10.3390/molecules27165087.
8. Singh, K., and Raparia, S. (2018). Fluorescence properties of some transition metal complexes of Schiff bases- A review. J. Anal. Pharm. Res. *7*, 500–502. https://doi.org/10.15406/japlr.2018.07.00274.
9. Fabbrizzi, L. (2020). Beauty in chemistry: Making artistic molecules with schiff bases. J. Org. Chem. *85*, 12212–12226. https://doi.org/10.1021/acs.joc.0c01420.
10. Memon, S., Memon, N., Mallah, A., Soomro, R., and Khuhawar, M. (2014). Schiff Bases as Chelating Reagents for Metal Ions Analysis. Curr. Anal. Chem. *10*, 393–417. https://doi.org/10.2174/1573411010003140521113731.
11. Gupta, K.C., and Sutar, A.K. (2008). Catalytic activities of Schiff base transition metal complexes. Coord. Chem. Rev. *252*, 1420–1450. https://doi.org/10.1016/j.ccr.2007.09.005.
12. Singh, S., Naik, T.S.S.K., Basavaraju, U., Khan, N.A., Wani, A.B., Behera, S.K., Nath, B., Bhati, S., Singh, J., and Ramamurthy, P.C. (2022). A systematic study of arsenic adsorption and removal from aqueous environments using novel graphene oxide functionalized UiO-66-NDC nanocomposites. Sci. Rep. *12*, 15802. https://doi.org/10.1038/s41598-022-18959-2.
13. Steele, D. (1991). Studies in analytical chemistry. Analytical absorption spectrophotometry in the visible and ultraviolet; The principles. Spectrochim. Acta A. *47*, 311. https://doi.org/10.1016/0584-8539(91)80105-r.
14. Picollo, M., Aceto, M., and Vitorino, T. (2019). UV-Vis spectroscopy. Phys. Sci. Rev. *4*, 20180008. https://doi.org/10.1515/psr-2018-0008.
15. Kan, C.C., Ibe, A.H., Rivera, K.K.P., Arazo, R.O., and de Luna, M.D.G. (2017). Hexavalent chromium removal from aqueous solution by adsorbents synthesized from groundwater treatment residuals. Sustain. Environ. Res. *27*, 163–171. https://doi.org/10.1016/j.serj.2017.04.001.
16. Dhal, B., Thatoi, H., Das, N., and Pandey, B.D. (2010). Reduction of hexavalent chromium by Bacillus sp. isolated from chromite mine soils and characterization of reduced product. J. Chem. Technol. Biotechnol. *85*, 1471–1479. https://doi.org/10.1002/jctb.2451.
17. Murphy, V., Tofail, S.A., Hughes, H., and McLoughlin, P. (2009). A novel study of hexavalent chromium detoxification by selected seaweed species using SEM-EDX and XPS analysis. Chem. Eng. J. *148*, 425–433. https://doi.org/10.1016/j.cej.2008.09.029.
18. Daneshvar, M., and Hosseini, M.R. (2018). Kinetics, isotherm, and optimization of the hexavalent chromium removal from aqueous solution by a magnetic nanobiosorbent. Environ. Sci. Pollut. Res. Int. *25*, 28654–28666. https://doi.org/10.1007/s11356-018-2878-1.
19. Bhattacharjee, S. (2016). DLS and zeta potential - What they are and what they are not? J. Control Release *235*, 337–351. https://doi.org/10.1016/j.jconrel.2016.06.017.
20. Sing, K.S.W., Everett, D.H., Haul, R.A.W., Moscou, L., Pierotti, R.A., Rouquerol, J., and Siemieniewska, T. (1985). Reporting Physisorption Data for Gas/Solid Systems with Special Reference to the Determination of Surface Area and Porosity. Pure Appl. Chem. *57*, 603–619. https://doi.org/10.1351/PAC198557040603/MACHINEREADABLECITATION/RIS.
21. Shim, J., Kumar, M., Mukherjee, S., and Goswami, R. (2019). Sustainable removal of pernicious arsenic and cadmium by a novel composite of MnO2 impregnated alginate beads: A cost-effective approach for wastewater treatment. J. Environ. Manage. *234*, 8–20. https://doi.org/10.1016/J.JENVMAN.2018.12.084.
22. Singh, S., Anil, A.G., Naik, T.S.K., Khasnabis, S., Khasnabis, S., Nath, B., Kumar, V., Subramanian, S., Singh, J., and Ramamurthy, P.C. (2022). Mechanism and kinetics of Cr(VI) adsorption on biochar derived from Citrobacter freundii under different pyrolysis temperatures. J. Water Proc. Eng. *47*, 102723. https://doi.org/10.1016/J.JWPE.2022.102723.
23. Javadian, H. (2014). Application of kinetic, isotherm and thermodynamic models for the adsorption of Co(II) ions on polyaniline/polypyrrole copolymer nanofibers from aqueous solution. J. Ind. Eng. Chem. *20*, 4233–4241. https://doi.org/10.1016/J.JIEC.2014.01.026.
24. Babapour, M., Hadi Dehghani, M., Alimohammadi, M., Moghadam Arjmand, M., Salari, M., Rasuli, L., Mubarak, N.M., and Ahmad Khan, N. (2022). Adsorption of Cr(VI) from aqueous solution using mesoporous metal-organic framework-5 functionalized with the amino acids: Characterization, optimization, linear and nonlinear kinetic models. J. Mol. Liq. *345*, 117835. https://doi.org/10.1016/J.MOLLIQ.2021.117835.
25. Guo, J., Li, J.J., and Wang, C.C. (2019). Adsorptive removal of Cr(VI) from simulated wastewater in MOF BUC-17 ultrafine powder. J. Environ. Chem. Eng. *7*, 102909. https://doi.org/10.1016/J.JECE.2019.102909.
26. Yang, Q., Zhao, Q., Ren, S., Lu, Q., Guo, X., and Chen, Z. (2016). Fabrication of core-shell Fe3O4@MIL-100(Fe) magnetic microspheres for the removal of Cr(VI) in aqueous solution. J. Solid State Chem. *244*, 25–30. https://doi.org/10.1016/J.JSSC.2016.09.010.
27. Niknam Shahrak, M., Ghahramaninezhad, M., and Eydifarash, M. (2017). Zeolitic imidazolate framework-8 for efficient adsorption and removal of Cr(VI) ions from aqueous solution. Environ. Sci. Pollut. Res. Int. *24*, 9624–9634. https://doi.org/10.1007/S11356-017-8577-5.
28. Yang, Z.H., Cao, J., Chen, Y.P., Li, X., Xiong, W.P., Zhou, Y.Y., Zhou, C.Y., Xu, R., and Zhang, Y.R. (2019). Mn-doped zirconium metal-organic framework as an effective adsorbent for removal of tetracycline and Cr(VI) from aqueous solution. Microporous Mesoporous Mater. *277*, 277–285. https://doi.org/10.1016/J.MICROMESO.2018.11.014.
29. Singh, S., Anil, A.G., Khasnabis, S., Kumar, V.V., Kumar, V., Adiga, V., Kumar Naik, T.S.S., Subramanian, S., Kumar, V.V., Singh, J., and Ramamurthy, P.C. (2022). Sustainable removal of Cr(VI) using graphene oxide-zinc oxide nanohybrid: Adsorption kinetics, isotherms and thermodynamics. Environ. Res. *203*, 111891.
30. Singh, S., Naik, T.S.S.K., Anil, A.G., Khasnabis, S., Nath, B., U, B., Kumar, V., Garg, V.K., Subramanian, S., Singh, J., and Ramamurthy, P.C. (2022). A novel CaO nanocomposite cross linked graphene oxide for Cr(VI) removal and sensing from wastewater. Chemosphere *301*, 134714. https://doi.org/10.1016/J.CHEMOSPHERE.2022.134714.
31. Wu, S., Ge, Y., Wang, Y., Chen, X., Li, F., Xuan, H., and Li, X. (2018). Adsorption of Cr(VI) on nano Uio-66-NH2 MOFs in water. Environ. Technol. *39*, 1937–1948. https://doi.org/10.1080/09593330.2017.1344732.
32. Yan, L., Guo, W., Huang, B., Chen, Y., Ren, X., Shen, Y., Zhou, Y., Cheng, R., Zhang, J., Qiu, M., and Hu, B. (2023). Efficient removal of Cr(VI) by the modified biochar with chitosan schiff base and MnFe2O4 nanoparticles: Adsorption and mechanism analysis. J. Environ. Chem. Eng. *11*, 109432. https://doi.org/10.1016/J.JECE.2023.109432.
33. Elhag, M., Abdelwahab, H.E., Mostafa, M.A., Nasr, A.Z., and El Sadek, M.M. (2020). Synthesis and characterization of chitosan-pyrazoloquinoxaline Schiff bases for Cr (VI) removal from wastewater. Int. J. Biol. Macromol. *163*, 2180–2188. https://doi.org/10.1016/J.IJBIOMAC.2020.09.090.
34. Anush, S.M., Chandan, H.R., and Vishalakshi, B. (2019). Synthesis and metal ion adsorption characteristics of graphene oxide incorporated chitosan Schiff base. Int. J. Biol. Macromol. *126*, 908–916. https://doi.org/10.1016/J.IJBIOMAC.2018.12.164.
35. Wei, Y., Wang, H., Zhang, X., and Liu, C. (2021). Ammonia-assisted hydrothermal carbon material with schiff base structures synthesized from factory waste hemicelluloses for Cr(VI) adsorption. J. Environ. Chem. Eng. *9*, 106187. https://doi.org/10.1016/J.JECE.2021.106187.
36. Boorboor Ajdari, F., and Behzad, M. (2016). Efficient adsorption of Cu(II) and Cr(VI) metal ions by Schiff base modified SBA-15. Appl. Chem. Today *10*, 97–105. https://doi.org/10.22075/CHEM.2017.726.
37. Xu, S., Huang, J., Wei, X., Chen, Y., Liu, M., Wu, J., and Liu, Y. (2024). Preparation of amine functionalized micro-mesoporous silicon adsorbent from fly ash and its kinetic characteristics of CO2 adsorption/desorption process. Ceram. Int. *50*, 25150–25160. https://doi.org/10.1016/J.CERAMINT.2024.04.244.
38. Yap, P.L., Nguyen, H.H., Ma, J., Gunawardana, M., and Losic, D. (2024). Exploring kinetic and thermodynamic insights of graphene related two dimensional materials for carbon dioxide adsorption. Sep. Purif. Technol. *348*, 127633. https://doi.org/10.1016/J.SEPPUR.2024.127633.
39. George, R., and Sugunan, S. (2014). Kinetics of adsorption of lipase onto different mesoporous materials: Evaluation of Avrami model and leaching studies. J. Mol. Catal. B Enzym. *105*, 26–32. https://doi.org/10.1016/J.MOLCATB.2014.03.008.
40. Sayed, H., Mahmoud, R., Mohamed, H.F., Gaber, Y., and Shehata, N. (2022). Co and Ni Double Substituted Zn-Fe Layered Double Hydroxide as 2D Nano-Adsorbent for Wastewater Treatment. Key Eng. Mater. *922*, 193–213. https://doi.org/10.4028/P-TPNS6C.
41. Bakar, S.A., Geedi, H.S., Khamidun, M.H., Mohamed, R.M.S.R., Daud, M.F.C., and Md Ali, U.F. (2023). Evaluation lead removal kinetics modelling of adsorption by using composite of Chitosan and Ceramic waste. IOP Conf. Ser. Earth Environ. Sci. *1205*, 012010. https://doi.org/10.1088/1755-1315/1205/1/012010.
42. Aljeboree, A.M., Radia, N.D., Jasim, L.S., Alwarthan, A.A., Khadhim, M.M., Washeel Salman, A., and Alkaim, A.F. (2022). Synthesis of a new nanocomposite with the core

TiO2/hydrogel: Brilliant green dye adsorption, isotherms, kinetics, and DFT studies. J. Ind. Eng. Chem. *109*, 475–485. https://doi.org/10.1016/J.JIEC.2022.02.031.

43. Nassar, H., Shaban, A., zaher, A., Abdelmonein, T., Salama, E., gaber, Y., Shehata, N., Abdelhameed, R., and Mahmoud, R. (2022). Iron-Trimesic Metal Organic Frameworks as Nano-Adsorbents for Tetracycline and Ceftriaxone Contaminated Wastewater Effluents. Egypt. J. Chem. *0*, 439–449. https://doi.org/10.21608/EJCHEM.2022.153568.6647.
44. Chen, X., Hossain, M.F., Duan, C., Lu, J., Tsang, Y.F., Islam, M.S., and Zhou, Y. (2022). Isotherm models for adsorption of heavy metals from water - A review. Chemosphere *307*, 135545. https://doi.org/10.1016/J.CHEMOSPHERE.2022.135545.
45. Çelik, M.S., Kütük, N., Yenidünya, A.F., Çetinkaya, S., and Tüzün, B. (2023). Removal of safranin O from wastewater using Streptomyces griseobrunneus dead biomass and in silico calculations. Biomass Convers. Biorefinery *1*, 1–12. https://doi.org/10.1007/S13399-023-04558-2.
46. Sismanoglu, S., Akalin, M.K., Akalin, G.O., and Topak, F. (2023). Effective Removal of Cationic Dyes from Aqueous Solutions by Using Black Cumin (Nigella sativa) Seed Pulp and Biochar. Bioresources *18*, 3414–3439. https://doi.org/10.15376/biores.18.2.3414-3439.
47. Busetty, S., Chandrasekaran, R., and Vedartham, S. (2021). Isotherm and Kinetic Modeling Analysis of Water Decontamination through Biosorption. Biosorption for Wastewater Contaminants, 117–146. https://doi.org/10.1002/9781119737629.CH7.
48. Blöchl, P.E., Jepsen, O., and Andersen, O.K. (1994). Improved tetrahedron method for Brillouin-zone integrations. Phys. Rev. B *49*, 16223–16233. https://doi.org/10.1103/PhysRevB.49.16223.
49. Giannozzi, P., Baroni, S., Bonini, N., Calandra, M., Car, R., Cavazzoni, C., Ceresoli, D., Chiarotti, G.L., Cococcioni, M., Dabo, I., et al. (2009). QUANTUM ESPRESSO: a modular and open-source software project for quantum simulations of materials. J. Phys. Condens. Matter *21*, 395502. https://doi.org/10.1088/0953-8984/21/39/395502.
50. Perdew, J.P., Burke, K., and Ernzerhof, M. (1996). Generalized Gradient Approximation Made Simple. Phys. Rev. Lett. *77*, 3865–3868.
51. Liechtenstein, A.I., Anisimov, V.I., and Zaanen, J. (1995). Density-functional theory and strong interactions: Orbital ordering in Mott-Hubbard insulators. Phys. Rev. B Condens. Matter *52*, R5467–R5470.
52. Grimme, S. (2006). Semiempirical GGA-type density functional constructed with a long-range dispersion correction. J. Comput. Chem. *27*, 1787–1799. https://doi.org/10.1002/jcc.20495.

STAR★METHODS

KEY RESOURCES TABLE

REAGENT or RESOURCE	SOURCE	IDENTIFIER
Chemicals, peptides, and recombinant proteins		
Thio carbohydrazide (99%)	Spectrochem Pvt. Ltd, India	Cat#0120343
Salicylaldehyde (98%)	Spectrochem Pvt. Ltd, India	Cat#011909
Glacial acetic acid (99.8%)	SD Fine Pvt. Ltd, India	Cat#37013
Potassium dichromate (99.9%)	SD Fine Pvt. Ltd, India	Cat#39605
Ethanol (99.8%)	Sigma-Aldrich	Cat#24102
Software and algorithms		
Origin Pro 2024b	Origin Lab	https://www.originlab.com/demodownload.aspx
DFT studies	QUANTUM Espresso software	https://www.quantum-espresso.org/
Microsoft EXCEL	Microsoft	https://www.microsoft.com/ja-jp/microsoft365/excel

METHOD DETAILS

Chemicals and solvents

Thio carbohydrazide (99%) and salicylaldehyde (98%), were supplied from Spectrochem Pvt. Ltd, India. Glacial acetic acid (99.8%), Potassium dichromate (99.9%), and ethanol (99%) were supplied from SD Fine Pvt. Ltd, India. Ethanol (99.8 %) was obtained from Sigma-Aldrich and implemented without any additional purification.

Material synthesis

The synthetic procedure for the Schiff base sorbent is illustrated in Scheme 1. A modified version of a previously reported method was used. An ethanolic suspension of thiocarbohydrazide (1 g, 9.42 mmol) was prepared, to which an ethanolic solution of 2-aminophenol (2.06 g, 18.84 mmol) was gradually added. Glacial acetic acid was used as a catalyst, and the reaction mixture was refluxed for 4 hours. The progress of the reaction was monitored using Thin Layer Chromatography (TLC). Upon completion, as indicated by TLC, the reaction mixture was filtered, and the precipitate was washed with cold water. The resulting product was dried at 60°C overnight, yielding a pale-yellow powder (2.4 g) with an 82% yield. This pale-yellow powder was subsequently used in the adsorption tests conducted in this study. ^{1}H NMR (DMSO-d_6, 400 MHz): δ, 6.91-6.93 (4H, m), 7.29-7.41 (3H, m), 8.08 (1H, s), 8.50-8.77 (2H, br), 10.04 (1H, s), 11.63 (1H, s), 11.89 -12.08 (2H, br). FTIR (ν, cm^{-1}) – 3700, 3200, 2703 (OH stretch), 3046 (-OH bonded stretch), 2950 (-NH stretch), 2128 (N-C=S stretch), and 1626 (N-H bending).

Material characterization

FT-IR spectra were collected using a Bruker Tensor II spectrophotometer. UV-visible absorbance spectra were recorded with a Perkin-Elmer Lambda 35 instrument. X-ray diffraction studies were conducted using a CCD-based single-crystal X-ray diffractometer. Proton NMR analysis was performed using a Bruker 400 MHz High-Resolution Multinuclear FT-NMR Spectrometer. Dynamic light scattering measurements were obtained with a Zetasizer Nano-series ZEN 3690 instrument from Malvern Instruments. Raman spectra were acquired using the STR-300 confocal Raman spectrometer from Seki Technotron Corp., featuring a diode laser excitation source (785 nm). The Raman scattering data were obtained using a 50x objective and a 600 lines/mm diffraction grating, with data gathered for 10 seconds with 12 accumulations, using a Peltier-cooled CCD detector.The morphological assessment of the Schiff base particles was carried out using a Zeiss Ultra-55 FE-SEM instrument from Carl Zeiss via Field Emission Scanning Electron Microscopy (FE-SEM), Germany. EDS investigations were conducted using the ZEISS ULTRA 55 instruments, coupled with scanning electron imaging. Textural characterization of the prepared Schiff base was performed by N_2 adsorption at 77 K using a BELSORP MAX-2 (Microtrac MRB), USA. The Brunauer–Emmett–Teller (BET) surface area, total pore volume, and pore size distribution of the prepared material were determined before and after Cr(VI) adsorption.

Kinetics & isotherms

The kinetic data of Cr (VI) adsorption onto Thiourea-Salicylaldehyde (TSA) were fitted by five kinetic models, i.e., intraparticle diffusion (IPD), Pseudo-1st-order, Pseudo-2nd -order, mixed 1st and 2nd -order, and Avrami models.[40–43] These models were given as follows:

$$\text{IPD}: q_t = k_{ip}\sqrt{t} + c_i p \quad \text{(Equation 1)}$$

$$\text{Pseudo} - 1^{st} - \text{order} : q_t = q_e\left(1 - \exp(-k_1 t)\right) \quad \text{(Equation 2)}$$

$$\text{Pseudo} - 2^{nd} - \text{order} : q_t = \frac{k_2 q_e^2 t}{1+k_2 q_e t} \quad \text{(Equation 3)}$$

$$\text{Mixed } 1^{st}, 2^{nd} - \text{order} : q_t = q_e \frac{1 - \exp(-kt)}{1 - f_2\ exp\ (-kt)} \quad \text{(Equation 4)}$$

$$\text{Avrami} : q_t = q_e\left[1 - \exp\left(-k_{av}t\right)^{nav}\right] \quad \text{(Equation 5)}$$

Where: q_t and q_e (mg g^{-1}) refer to the adsorption capacity of Cr (VI) at time t and equilibrium time, respectively, c_{ip} (mg g^{-1}), k_1 (min^{-1}), k_2 (gmg^{-1} min^{-1}), k ($mg.g^{-1}$ min^{-1}), k_{av} (min^{-1}) and are the IPD, Pseudo-1^{st} -order, Pseudo-2^{nd} -order, mixed 1^{st} , 2^{nd} -order, and Avrami models constants, f_2 (-) and k_{ip} (mg g^{-1} $min^{-1(1/2)}$) are the mixed 1^{st} and 2^{nd} -order, and IPD coefficients, n_{av} (-) is Avrami component.

Adsorption modelling

To comprehend how the Cr (VI) adsorbed onto the TSA as well as to determine the maximum adsorption capacity (q_{max}) of the TSA, eleven isotherm models, i.e. Freundlich, Langmuir, Dubinin–Radushkevich, Langmuir-Freundlich, Sips, Temkin, Redlich-Peterson, Toth, Khan, Baudu and Fritz-Schlunder[44–47] have been investigated. These models were given as follows:

$$\text{Langmuir} : q_e = q_{max}\frac{K_L\ Ce}{1+K_L\ Ce} \quad \text{(Equation 6)}$$

$$\text{Freundlich} : q_e = K_f\ C_e^{1/n} \quad \text{(Equation 7)}$$

$$\text{Dubinin–Radushkevich} : q_e = q_{max}\exp\left(-K_{DR}\ \epsilon^2\right) \quad \text{(Equation 8)}$$

$$\text{Langmuir} - \text{Freundlich} : q_e = \frac{q_{max}\ (K_{LF}C_e)^{MLF}}{1+(K_{LF}C_e)^{MLF}} \quad \text{(Equation 9)}$$

$$\text{Sips} : q_e = \frac{q_{max}K_s(C_e)^{1/ns}}{1+K_s(C_e)^{1/ns}} \quad \text{(Equation 10)}$$

$$\text{Redlich} - \text{Peterson} : q_e = \frac{K_R C_e}{1+a_R C_e^{\beta R}} \quad \text{(Equation 11)}$$

$$\text{Toth} : q_e = \frac{K_T C_e}{\left(a_T+C_e^Z\right)^{1/Z}} \quad \text{(Equation 12)}$$

$$\text{Khan} : q_e = \frac{q_{max}b_K C_e}{(1+b_K C_e)^{aK}} \quad \text{(Equation 13)}$$

$$\text{Baudu} : q_e = \frac{q_{max}\ bo\ C_e^{1+x+y}}{1+bo\ C_e^{1+x}} \quad \text{(Equation 14)}$$

$$\text{Fritz} - \text{Schlunder} : q_e = \frac{q_{max}\ K_1 C_e^{m1}}{1+K_2 C_e^{m2}} \quad \text{(Equation 15)}$$

Where: C_e is the concentration of Cr (VI) at equilibrium in solution, K_L (L mg^{-1}) is Langmuir isotherm constant, M_{LF} is heterogeneous parameter and it lies between 0 and 1, K_{LF} is equilibrium constant for heterogeneous solid, n and K_F (L mg^{-1}) are the coefficients related to strength constants and adsorption capacity according to Freundlich isotherm model, respectively, k_s is Sips isotherm constant; ns is Sips isotherm model exponent also named as heterogeneity factor, K_{DR} (mol^2 Kj^{-2}) is Dubinin–Radushkevich isotherm constant; ε (kJ mol^{-1}) is Polanyi potential, K_T (mg g^{-1}) and aT (mg L^{-1}) are Toth constants, z refers to the degree of heterogeneity of the adsorption systems, K_R and a_R are Redlich-Peterson constants; β_R is the exponent that can be lied between 0 and 1, while K_1, K_2, m_1 and m_2 are Fritz-Schlunder parameters.

Density functional theory studies

Here, the density functional theory (DFT) based on initio simulations for Schiff's base system are performed via projector augmented wave formalism[48] using QUANTUM Espresso software.[49] Perdew-Burke-Ernzerhof (PBE) generalized gradient approximation (GGA) is considered to describe the exchange and correlation functional.[50] Here, 480 eV is set as the plane-wave cut off energy value and taken approximately 20 Å as vacuum space in the simulation box to minimize adjacent slab interaction. A Monkhorst-Pack (MP) grids is used of 9 × 9 × 9 supercell with first Brillouin zone integration for structural relaxation and a denser MP grid of 27 × 27 × 27 for electronic structure calculations. The van der Waals (vdWs) corrections are implemented including Grimme (DFT-D2) method[51,52] in this simulation.

The TSA Schiff's base ($C_{14}H_{14}N_4O_2S$) molecule has been optimized in a 3 × 3 × 3 $Å^3$ unit cell. Its adsorption on the surfaces has been modelled using 2 × 2 × 2 (for Cr (VI) ion) supercell with four atomic layers of potassium dichromate (VI) ($K_2Cr_2O_7$) slab. This gives a total of 82 atoms for the slab and 24 atoms for the adsorbate with 20 Å of vacuum. Cr atom takes +6 oxidation state in $K_2Cr_2O_7$ as a result Cr (VI) ionic state can be designed in the calculations. The slab layers have been undergone volume relaxation in the bulk-phase structure. The stable configuration of potassium dichromate has been determined by exhausting a number of possible orientations of the TSA Schiff's base molecule on the slab surface such as the *S*-up (Figure 1A), *S*-down (Figure 1B), parallel (Figure 1C), and vertical (Figure 1D) orientations with rotation about the Z-axis. In this figure, the naming of orientations is based on the initial configuration of TSA Schiff's base molecule prior to optimization. After relaxation, it has been noticed that the molecule has shifted into configurations that are not perfectly vertical (perpendicular) nor parallel to the slab surface.

QUANTIFICATION AND STATISTICAL ANALYSIS

In the manuscript, all adsorption data presented are derived from the mean values of triplicate experimental readings. The statistical analysis and data processing were conducted utilizing OriginPro 2024b Learning Edition software. This software enabled the precise calculation of mean values and facilitated comprehensive data analysis, ensuring robustness and accuracy in the reported adsorption metrics. Each data point reflects the average of three independent measurements, with the variation and standard deviation quantified to provide a measure of reproducibility and reliability.